Scanning electron-acoustic microscopy of MgO crystals

M. Urchulutegui, J. Piqueras, and J. Llopis
Departamento de Fisica de Materiales, Facultad de Fisicas, Universidad Complutense, 28040, Madrid, Spain

(Received 28 September 1988; accepted for publication 11 November 1988)

The capability of scanning electron-acoustic microscopy in the characterization of MgO crystals has been studied. The conditions for the observation of different surface and subsurface features in as-grown and deformed crystals are described and the results are discussed on the basis of thermal and nonthermal mechanisms of acoustic signal generation.

INTRODUCTION

Scanning electron-acoustic microscopy (SEAM), also referred to as thermal wave microscopy, was developed in 1980[1,2] and has been used in the last years in the characterization of many materials. Some recent reviews[3–5] describe a number of SEAM applications which refer mainly to metals and semiconductors, as well as to the detection of subsurface features in different samples. Few[6] SEAM observations of ionic crystals have been reported although this technique can be used to detect features such as cracks, deformed regions, precipitates, bubbles, etc., often present in this kind of crystal. The present work is a preliminary study of the capabilities of SEAM in the characterization of MgO single crystals. The capabilities would be, in principle, similar for other ceramic materials. The influence of some experimental parameters on SEAM images is described. Some observations are briefly compared with previous[7–9] SEM cathodoluminescence observations on MgO crystals.

EXPERIMENTAL METHOD

The MgO single crystals used were grown by W. & C. Spicer with purity of 99.9% or 99.99%. The crystals were cleaved along (100) faces. Some samples were indented with loads between 20 and 200 g with a diamond pyramid by using the MHP microhardness attachment of a Zeiss optical microscope. The samples were coated with a transparent carbon film. Cathodoluminescence and scanning electron-acoustic observations of the samples were performed on a Cambridge S4-10 scanning electron microscope. The experimental method for CL measurements in the range 350–850 nm has been previously described.[10]

The experimental SEAM arrangement used in this work (Fig. 1) is similar to those previously used by other authors. The chopping system consists of a pair of condensor plates and beam blanking electronics to create a periodic beam. A function generator (Tektronix FG-504) was used to produce a square-wave voltage with frequencies up to 240 kHz. The sound signal is detected by a piezoelectric ceramic transducer which is clamped to the bottom of the specimen. The specimen-transducer assembly used is similar to that described by Balk and Kultscher.[11] The amplification is carried out by a low-noise preamplifier (Ithaco 1201), a lock-in amplifier (Ithaco 393) receiving the reference signal from the function generator, and a video amplifier (Tektronix AM-502). With the amplitude A and the phase delay ϕ of the detected signal with respect to the reference square wave, alternative images corresponding to A, $A \sin \phi$, or $A \cos \phi$ can be formed. The acoustic signal was detected at the reference frequency f or at $2f$.

RESULTS AND DISCUSSION

The SEM images of the crystals in the emissive mode show, in general, only surface steps and occasionally, in chemically polished crystals, rounded features of a size of several micrometers. Etching the crystals reveals the presence of subgrain boundaries that are also readily observed in the SEM-cathodoluminescence image.[12] Figure 2 shows the SEAM image of subboundaries. CL observations[12] indicate

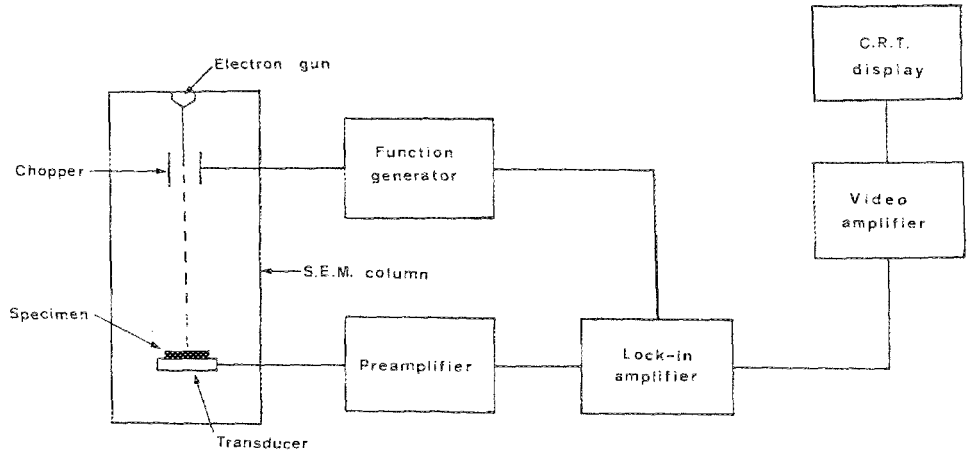

FIG. 1. Schema of the SEAM system.

 0021-8979/89/072677-04$02.40

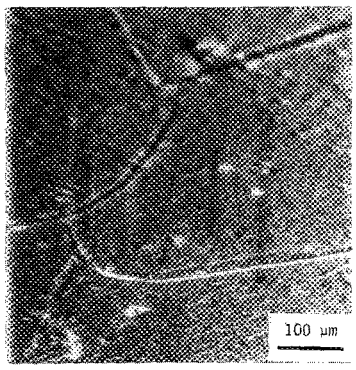

FIG. 2. SEAM image of subgrain boundaries.

the presence of a defect concentration gradient near the subboundary. The bright bands at the sides of the boundary in Fig. 2 could be related to this effect. The SEAM generation mechanism is typically explained by the conversion of an electron-beam-induced heat distribution into sound by means of the thermal expansion coefficient (thermal wave model)[13] but evidence has been found[14] of other nonthermal mechanisms (piezoelectric coupling, excess carrier coupling in semiconductors). In the thermal wave model the resolution of the SEAM image is proportional to $\omega^{-1/2}(\omega = 2\pi f)$. Such dependence has been found in metals.[15,16] In particular, it has been found in Ref. 16 that the grain-boundary width in the SEAM image shows the dependence $\omega^{-1/2}$. It has been observed in the present work that increasing the frequency from 50 to 240 kHz causes the reduction of the acoustic signal but not significant changes in the width of the SEAM subboundary image are detected. This suggests that other signal generation mechanisms can act in addition to thermal coupling. On the other hand, chemical etching facilitates the observation of the subboundary which indicates that a surface effect is involved in the image. However, other surface features clearly observed in the emissive mode do not appear in the SEAM image as Fig. 3 shows. In the SEAM image only subsurface features are observed whose appearance depends on experimental parameters as frequency, phase angle of the signal with respect to the electron beam, and electron-beam energy. The nature of these features has not been determined but their subsurface character makes them useful to study the SEAM capabilities. By decreasing the frequency [Figs. 3(b) and 3(c)] the image becomes somewhat less sharp but new features marked A in the micrograph scarcely visible at 220 kHz appear in the 50-kHz image. The decrease of the chopping frequency causes an increase of the thermal decay length d_t. Both quantities are related by $d_t = (2K/\omega\rho C)^{1/2}$ where ρ is the density, C the specific heat capacity, and K the thermal conductivity. d_t determines the specimen volume in which thermal generation of acoustic signal is produced. In the case of MgO the d_t values at 220 and 50 kHz are about 4 and 8 μm, respectively. According to that, the features emerging at low frequencies would be situated deeper in the sample.

When the beam energy is increased from 20 to 30 keV, changes are observed in the SEAM image [Figs. 3(c) and 3(d)] that are probably related to a higher mean signal generation depth at 30 keV. Comparison of Figs. 3(b), 3(c), and 3(d) shows that increasing the beam energy from 20 to 30 keV influences the SEAM image more than changing the chopping frequency. This result could be explained if the electron range at 30 keV is higher or at least comparable to the values of d_t at frequencies between 50 and 240 kHz. Another possibility is that d_t has only a small influence on the image because the SEAM contrast is not only due to a thermal mechanism but also nonthermal[14] signal generation mechanisms are involved. In some nonthermal mechanisms[14] the maximum volume being responsible for the sound generation would be a slightly enlarged primary ener-

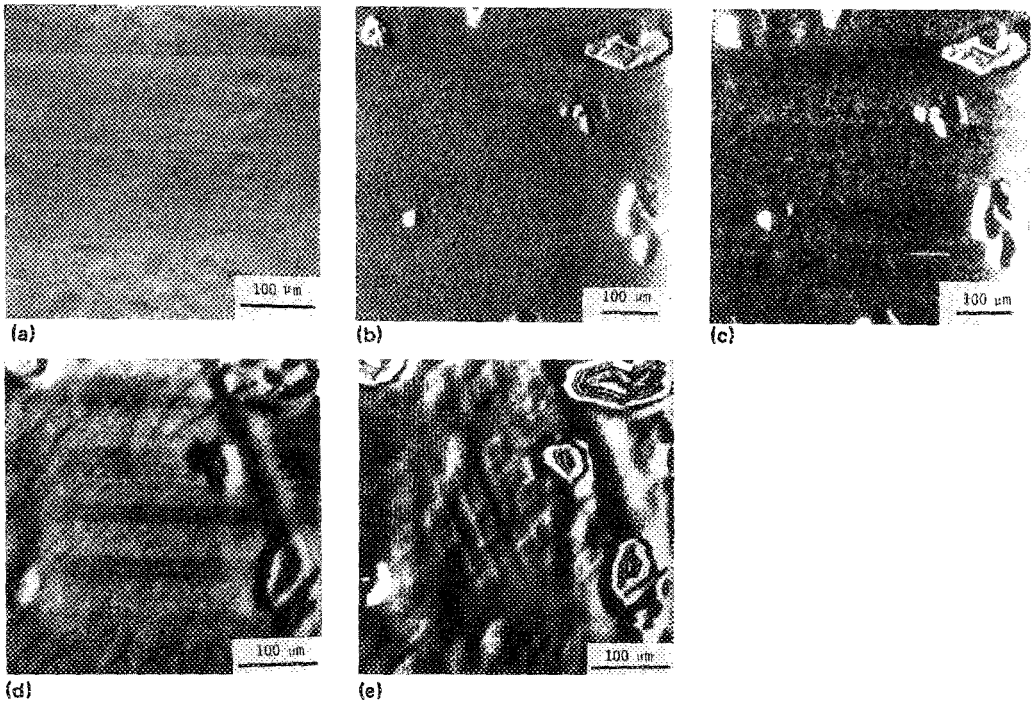

FIG. 3. Undeformed sample. (a) Secondary electron image, (b) linear SEAM amplitude image at 220 kHz and 20 keV, (c) linear SEAM amplitude image at 50 kHz and 20 keV, (d) linear SEAM amplitude image at 50 kHz and 30 keV, and (e) nonlinear ($2f$) SEAM amplitude image at 100 kHz.

gy dissipation volume. In MgO the electron range increases from about 2.4 μm at 20 keV to 5 μm at 30 keV.[17] Since the electron range values are lower than d_t, it does not seem that the high influence of the electron-beam energy on the SEAM image can be explained by a thermal coupling alone. It rather suggests the existence of nonthermal, in addition to thermal, mechanisms. The influence of electron-beam energy on the SEAM image of different materials has been previously investigated. Balk *et al.*[15] in a Cu-Zn-Al alloy have not found significant variation of SEAM contrast at 100 kHz between 7 and 30 keV, which agrees with the fact that in metals d_t is several times higher than the electron range and that the variation of spatial resolution with frequency can be explained by thermal coupling. A similar result regarding the beam energy has been found by Holstein[18] in an alumina fiber/aluminum matrix composite while in semiconductors and semiconductor devices[11,19] the SEAM image depends clearly on beam energy, which indicates that in semiconductors, the signal is due to the space-charge effect rather than to the thermoelastic effect.

The region shown in Fig. 3 has also been observed using the signals $A \sin \phi$ or $A \cos \phi$ but not better images or new details have been found under these conditions. On the contrary new features appear when the nonlinear[11] observation mode is used. Nonlinear processes in the signal generation mechanism lead to signals at harmonics of the chopping frequency. By tuning the detector frequency to $2f$ nonlinear images are obtained that can show improved spatial resolution and a contrast unattainable with the linear technique.[11,15,20] The nonlinear image [Fig. 3(e)] shows some straight lines, possibly related to deformed regions, and a ring contrast not observed in the linear mode. The width of some of the rings is about 1 μm, indicating a high spatial resolution of the nonlinear mode. A ring contrast has been previously observed[15,20] in the nonlinear images of the alloy Cu-Zn-Al around the end of martensite plates. In Ref. 20 a mechanism based in the microscopic dynamical, cyclic growth and shrinkage of the plates under the periodic influence of the chopped beam has been proposed to explain the ring contrast. The model is based on the thermoelastic behavior of the martensite and there is no reason to think that it can be applied to the features, with appearance of inclusions or precipitates observed in this work. It seems possible that, as suggested in Ref. 15, the rings represent strain contours of some sort and in that case the nonlinear images would allow a highly sensitive detection of the stress or strain situations in crystals.

The SEAM images of an indent are rather similar to the emissive mode images [Figs. 4(a) and 4(b)] but the former change with the parameters of the electroacoustic experiment. For instance, by decreasing the frequency, information from deeper regions of the specimen is obtained, as a comparison of Figs. 4(b) and 4(c) shows. In micrograph 4(c), taken at lower frequency, the line marked *B*, not visible in the other micrographs, is observed. As mentioned above, this effect can be explained by the dependence of the thermal decay length with ω and indicates the existence of thermal coupling. Decreasing the frequency causes, on the other side, a clear loss of spatial resolution as is to be expected when thermal coupling is present.

Figure 4(d) shows the CL image of the same indent. CL contrast of deformed MgO is due to a high light emission in the plastically deformed regions.[7–9] Comparison of Figs. 4(c) and 4(d) shows that the two imaging techniques, CL and SEAM, give different information on the imaged region. In Fig. 4(d) the contrast of the plastically deformed zone is higher but region *B* of Fig. 4(c) is not observed because *B* is either not a luminescent region or is too deep in the sample to be detected by CL.

It is concluded from the observations of the present work that SEAM can be used in the investigation of subsurface features in as-grown and indented MgO crystals. The results cannot be explained only by a thermal mechanism of acoustic signal generation but also nonthermal mechanisms have to be considered. The use of CL and SEAM in the same SEM appears to be useful for a better microcharacterization of the material.

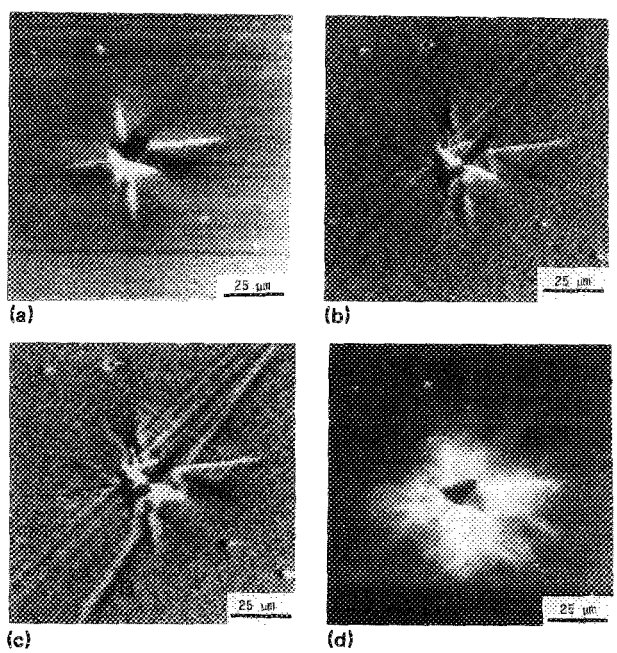

FIG. 4. Indented sample. (a) Secondary electron image, (b) SEAM amplitude image at 100 kHz, (c) SEAM amplitude image at 70 kHz and (d) CL image.

ACKNOWLEDGMENTS

This work has been supported by the Volkswagen Foundation and by the Comisión Interministerial de Ciencia y Tecnología (Project PB86-0151). The assistance of the Department of Materials for Electrical and Electronic Engineering of the University of Duisburg (G.F.R.) has made possible the development of the SEAM technique in our laboratory. Special thanks are due to Professor E. Kubalek and Dipl. Phys. N. Kultscher. The help of P. Fernández in this work is acknowledged.

[1] E. Brandis and A. Rosencwaig Appl. Phys. Lett. **37**, 98 (1980).
[2] G. S. Cargill, Nature **286**, 691 (1980).
[3] A. Rosencwaig, Annu. Rev. Mater. Sci. **15**, 103 (1985).

[4]L. J. Balk, Can. J. Phys. **64**, 1238 (1986).
[5]D. G. Davies, Philos. Trans. R. Soc. London Ser. A **320**, 243 (1986).
[6]D. G. Davies, Scanning Electron Microsc. **III**, 1163 (1983).
[7]J. Llopis, J. Piqueras, and L. Brú, J. Mater. Sci. **13**, 1361 (1978).
[8]J. Piqueras, J. Llopis, and L. Delgado, J. Appl. Phys. **52**, 4341 (1981).
[9]C. Ballesteros, J. Llopis, and J. Piqueras, J. Appl. Phys. **53**, 3201 (1982).
[10]J. Llopis and J. Piqueras, J. Appl. Phys. **54**, 4570 (1983).
[11]L. J. Balk and N. Kultscher, Ins. Phys. Conf. Ser. **67**, 387 (1983).
[12]J. Llopis and J. Piqueras, Phys. Status Solidi A **49**, K9 (1978).
[13]J. Opsal and A. Rosencwaig, J. Appl. Phys. **53**, 4240 (1982).
[14]N. Kultscher and L. J. Balk, Scanning Electron Microsc. **I**, 33 (1986).
[15]L. J. Balk, D. G. Davies, and N. Kultscher, Phys. Status Solidi A **82**, 23 (1984).
[16]J. C. Murphy, J. W. Maclachlan, and L. C. Aamodt, IEEE Trans. Ultrason. Ferroelectr. Freq. Control. **UFFC-33**, 529 (1986).
[17]A. Remón, J. Piqueras, J. Llopis, and C. Ballesteros, Phys. Status Solidi A **77**, K29 (1983).
[18]W. L. Holstein, J. Electron Microsc. Tech. **5**, 91 (1987).
[19]T. Ikoma, M. Murayama, and K. Morizuka, Jpn. J. Appl. Phys. **23**, Suppl. 23-1, 194 (1983).
[20]L. J. Balk, D. G. Davies, and N. Kultscher, Scanning Electron Microsc. **III**, 1601 (1984).